JGR Atmospheres

RESEARCH ARTICLE
10.1029/2019JD031023

Ice Core $\delta^{18}O$ Record Linked to Western Arctic Sea Ice Variability

Stacy E. Porter[1], Ellen Mosley-Thompson[1,2], and Lonnie G. Thompson[1,3]

[1]Byrd Polar and Climate Research Center, The Ohio State University, Columbus, Ohio, USA, [2]Department of Geography, Atmospheric Sciences Program, The Ohio State University, Columbus, Ohio, USA, [3]School of Earth Sciences, The Ohio State University, Columbus, Ohio, USA

Key Points:
- Stable isotopes from the Bona-Churchill ice core provide a millennial scale history of western Arctic climate variability and sea ice cover.
- Storm trajectories influence the isotopic composition and establish the connection between the Bona-Churchill site and the Bering Sea.
- Isotopic enrichment during the Little Ice Age suggests a warm Arctic/cold continents pattern and a shift in the prevailing storm tracks.

Supporting Information:
- Supporting Information S1

Correspondence to:
S. E. Porter,
porter.573@osu.edu

Citation:
Porter, S. E., Mosley-Thompson, E., & Thompson, L. G. (2019). Ice core $\delta^{18}O$ record linked to Western Arctic sea ice variability. *Journal of Geophysical Research: Atmospheres*, *124*. https://doi.org/10.1029/2019JD031023

Received 15 MAY 2019
Accepted 26 SEP 2019

Abstract Stable oxygen isotopes ($\delta^{18}O$) in the Bona-Churchill (B-C) ice core from southeast Alaska provide a valuable, high-resolution history of climate variability and sea ice cover in the western Arctic over the last 800 years. Multiple ice cores have been collected from the Wrangell-St. Elias Mountain Range; however, their $\delta^{18}O$ records exhibit little consistency as each core offers a unique view on local, regional, and/or global climate variability. To explore the primary mechanisms influencing the isotopic signature at the B-C site, we utilize isotope-enabled model data, reanalysis data, and observations, which all indicate a strong connection between isotopes at the B-C site and western Arctic climate, likely established by the location of the storm track in this region. Enriched B-C $\delta^{18}O$ reflects increased southerly flow and warmer waters in the Bering Sea, which modulates the heat flux through the Bering Strait and into the Arctic, thereby affecting sea ice cover in the western Arctic. The B-C $\delta^{18}O$ paleorecord shares some remarkable similarities ($r = -0.80$, $p < .001$) with the duration of western arctic sea ice cover reconstructed from a Chukchi Sea sediment core. Interestingly, during the Little Ice Age, enriched $\delta^{18}O$ and reduced western Arctic sea ice are observed and may be indicative of prolonged periods of the warm Arctic/cold continents pattern and a northwestward shift of the North Pacific storm track.

Plain Language Summary The Bona-Churchill (B-C) ice core from southeast Alaska provides a valuable, high-resolution history of climate variability and sea ice cover in the western Arctic over the last 800 years. In the polar regions, ice core–derived stable oxygen isotopes typically serve as a temperature proxy. However, isotopic records from ice cores collected from the mountainous regions of northwestern North America exhibit little relation to local temperatures, and few similarities exist among the ice core records. Modeled and observed data in this study suggest a link between isotopic variability in the Bona-Churchill (B-C) ice core and climate variability in the Bering Sea, possibly through the position of the North Pacific storm track. The high-resolution B-C isotope record provides a rare millennial history of climate variability and sea ice cover in the western Arctic. A prominent feature in the B-C isotopic record includes enrichment during the Little Ice Age, suggesting warmer conditions in the western Arctic, which likely resulted from a prolonged presence of the warm Arctic/cold continents pattern and an accompanying shift in storm trajectories.

1. Introduction

Climate variability in the Pacific Basin influences global temperatures (Kosaka & Xie, 2016; Meehl et al., 2013) and has far-reaching impacts extending into the Arctic (Lee et al., 2017; Screen & Francis, 2016). Atmospheric circulation can influence sea ice cover, and likewise, variability in sea ice cover can feedback onto the atmospheric circulation through changes in the surface heat flux, which alter the meridional temperature gradient (Liu et al., 2007). The influence of sea ice and snow cover on the overlying atmospheric circulation is stronger in the Pacific sector than in the Atlantic (Dethloff et al., 2006). Yet, the multidecadal nature of Pacific climate variability prohibits the relatively short instrumental records from capturing low-frequency climate variations and their influence on Arctic sea ice. Numerous paleorecords from northwest Canada and Alaska have been used to study climate variability of the Pacific and the Arctic on interannual to interdecadal timescales, yet the complex terrain of this region can greatly complicate the interpretation of these records (Figure 1). For example, the seasonality of precipitation, which is important for interpreting ice core records, varies greatly across the climate divisions of Alaska. Coastal stations along the Gulf of Alaska

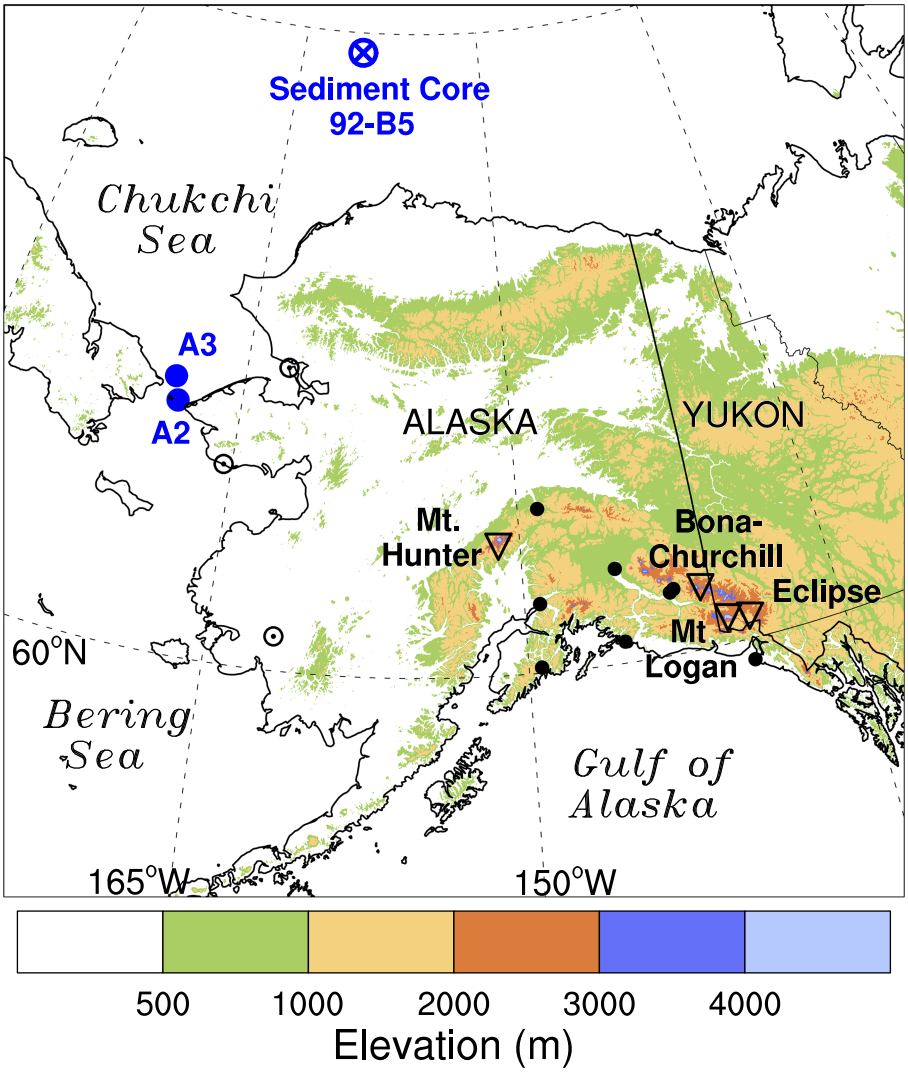

Figure 1. Topographical map showing the locations of the B-C ice core drill site and three other ice cores (triangles) and one marine sediment core. Bering Strait mooring observation sites (A2 and A3) and meteorological stations for the local (filled black circles) and western (open black circles) temperature composites are also shown.

receive the bulk of their precipitation in autumn, while stations in the interior receive much less precipitation overall due to the coastal topography and exhibit a precipitation maximum in summer (Bieniek et al., 2012). Winter precipitation is dominated by the Aleutian Low, a semipermanent low pressure system which reflects the intensity and location of the North Pacific storm track as well as the stationary wave pattern (Overland et al., 1999; Rodionov et al., 2007). Storms entering the Gulf of Alaska outnumber storms in the Bering Sea, which is considered a secondary storm track (Bieniek et al., 2011; Whittaker & Horn, 1984). In spring and summer, the Aleutian Low weakens and the storm track shifts northward (Fleming et al., 2000; Whittaker & Horn, 1984). Storm counts in the Gulf of Alaska and Bering Sea are relatively equivalent, although lower in both regions than in winter (Bieniek et al., 2011). Wetter summers in the interior occur when air is transported from the southwest rather than the south and southeast where the coastal topography contributes to moisture depletion (Streten, 1974). Summertime convection also contributes to precipitation in the interior (Fleming et al., 2000; Streten, 1974). This spatial and seasonal heterogeneity in precipitation determines how paleo-proxies preserve various climate phenomena.

Ice core-derived accumulation and sodium (Na^+) records have been extensively investigated as indicators of North and Tropical Pacific climate variability (Moore et al., 2001, Moore, Alverson, et al., 2002, Moore,

Holdsworth, et al., 2002, 2003; Rupper et al., 2004), meridional flow over the Gulf of Alaska (Kelsey et al., 2012), and strength of the Aleutian Low (Osterberg et al., 2014, 2017; Winski et al., 2017). Accumulation from the Mt. Logan ice core has been tied to local large-scale climate oscillators like the Pacific Decadal Oscillation (Moore, Alverson, et al., 2002, Moore, Holdsworth, et al., 2002) and tropical variability associated with the El Niño-Southern Oscillation (Moore et al., 2001, 2003). However, the connection between Mt. Logan accumulation and atmospheric circulation is only discernible in winters with high accumulation (Rupper et al., 2004). Accumulation on Eclipse Dome increases with strong southerly flow over the region (Kelsey et al., 2012). In the central interior of Alaska, an ice core from Mt. Hunter has exhibited increased accumulation since ~1840 CE, which has been attributed to a strengthening of the Aleutian Low (Winski et al., 2017). Likewise, Na^+ records from Mt. Hunter and Mt. Logan have been used to reconstruct Aleutian Low variability (Osterberg et al., 2014, 2017) such that increased storminess from a stronger Aleutian Low transports more sea salt to both ice core sites.

The stable isotopic composition ($\delta^{18}O$) of ice typically serves as a first-order proxy for temperature, particularly in the polar regions (Dansgaard, 1954, 1964; Johnsen et al., 1972). However, the $\delta^{18}O$ records from the aforementioned cores and other paleo-isotope records from this region exhibit little consistency (Kaufman et al., 2016). Characteristics of $\delta^{18}O$ in this region vary greatly with elevation (Holdsworth et al., 1991), and the complex mountainous topography has been shown to influence $\delta^{18}O$ in precipitation (Bailey et al., 2019). Due to its high elevation (5,340 m above sea level, masl), $\delta^{18}O$ from the Mt. Logan core is more closely associated with moisture source characteristics than local temperature (Fisher et al., 2004, 2008) similar to observations from Mt. Wrangell (Moore et al., 2016). Depleted $\delta^{18}O$ on Mt. Logan indicates southerly advection of moisture from more distant sources including the Tropics especially during an El Niño event, while enriched $\delta^{18}O$ indicates more zonal flow and local moisture sources (Fisher et al., 2004, 2008). The Eclipse (3,017 masl) $\delta^{18}O$ record, however, provides a stronger indicator of local temperature than Mt. Logan $\delta^{18}O$ (Wake et al., 2002), such that extremely enriched (depleted) $\delta^{18}O$ on Eclipse occurs when warm southerly flow increases (decreases; Kelsey et al., 2012). Modeling and observational studies also suggest isotopic enrichment with enhanced southerly flow due to a strengthened Aleutian Low (Bailey et al., 2015; Field et al., 2010).

The contradictory nature of these $\delta^{18}O$ interpretations suggests that although each paleorecord may offer a unique view on local, regional, or global climate variability, caution should be employed in multiproxy composite paleo-reconstructions of climate in this region until the individual records have been thoroughly explored and better understood. In 2002, the Bona-Churchill (B-C) ice core was drilled to bedrock (460.96 m) from the col between Mt. Bona and Mt. Churchill (61.4°N; 141.7°W; 4,420 masl) in the Wrangell-St. Elias Mountain Range in southeastern Alaska (Figure 1). On the col, the 10-m borehole temperature was −23 °C which approximates the average annual temperature (Cuffey & Paterson, 2010), and only a few very thin (~1 mm) melt layers were observed throughout the core (Text S1). The average annual layer thickness is 1.38 m water equivalent (w.e.) from 1971 to 2000 CE, the standard climatological mean period. The B-C site is ~150 km northwest of the Mt. Logan and Eclipse ice core drill sites; however, the elevation of the B-C site (4,420 masl) is between those of Mt. Logan and Eclipse. Here we present the B-C $\delta^{18}O$ record over the last 800 years and explore the primary mechanisms influencing $\delta^{18}O$ on this intermediate elevation icefield.

2. Data and Methods

2.1. Bona-Churchill Ice Core

The entire length of the B-C core was cut into three sets of 12,161 discrete, coregistered samples that were analyzed for the concentration and size distribution of insoluble dust particles, the oxygen ($\delta^{18}O$) and hydrogen (δD) isotopic composition, and the concentrations of major anions and cations preserved in the ice (see Text S1 for analytical details). To facilitate identification of a seasonally varying constituent (e.g., dust concentration), 10 to 15 samples are typically cut from the average annual layer thickness. As the annual layers thin with depth in the core, the sample lengths are reduced accordingly. For the upper 10 m of the B-C core the average sample size was 0.115 m, which was slowly reduced to 0.016 m for the bottom 30 m of the core (Text S1). Individual years were delineated by annual dust peaks which generally occur in spring, such that the annual layer roughly approximates the thermal year (July–June). Above 100 m in the core, the annual

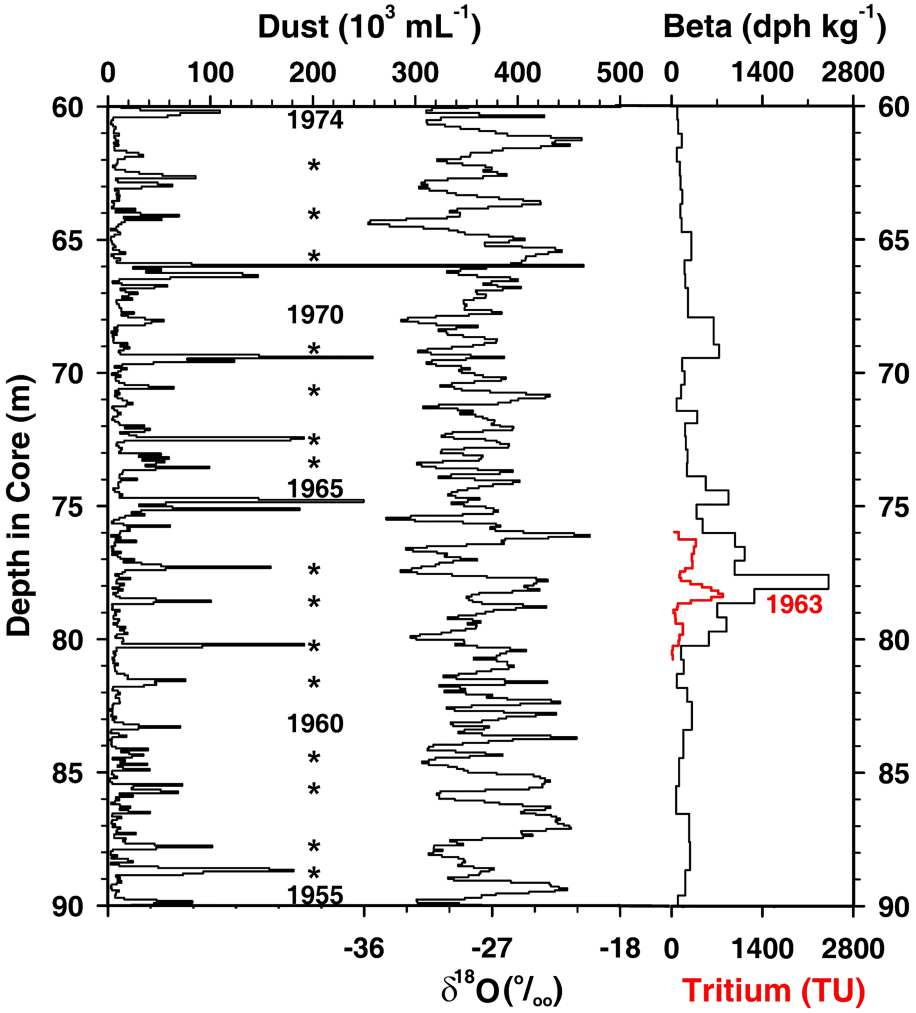

Figure 2. Timescale development for B-C ice core. Individual sample values for insoluble dust concentration and $\delta^{18}O$ are shown along with beta radioactivity, reflecting ^{137}Cs and ^{90}Sr concentrations, and the abundance of tritium (^{3}H) in the ice core section from 60 to 90 m depth that is dated from 1955 to 1974 CE (asterisks represent annual demarcations) using only seasonal variations in dust content. Tritium measurements were made by Ulrich Schotterer at the University of Bern, Switzerland. Annual average $\delta^{18}O$ for the upper 400 meters used in this study are shown in Figure S3.

average $\delta^{18}O$ values were determined using the annual layers delineated solely by the dust peaks as the $\delta^{18}O$ profile exhibits subannual variations that likely reflect preservation of individual precipitation events (Figure 2). During the densification process, snow is metamorphosed into firn and eventually into ice, and concomitantly diffusional smoothing reduces or removes high-frequency variations which often make the annual $\delta^{18}O$ signal more discernible (Figure S1). However, diffusion can also introduce artifacts that may be misinterpreted as annual signals and over time the true annual variations are typically diminished and eventually may disappear at greater depths (Johnsen, 1977; Johnsen et al., 2000). The diffusion length for a site is the maximum distance that a water molecule has moved from its original stratigraphic position and depends primarily on the accumulation rate and the temperature and density profiles (Laepple et al., 2018). For B-C the estimated diffusion length of 0.10 to 0.15 m w.e. is much smaller than the average annual layer thickness (1.38 m w.e. or ~2.13 m of snow), which is comparable to ~13 cm determined for the Renland ice cap in east Greenland (Holme et al., 2019). Thus, the effect of diffusional smoothing of $\delta^{18}O$ over much of the B-C ice core is primarily to reduce subannual variability so that using the annual signal in $\delta^{18}O$ for intermittent dating support only when the annual dust signal is questionable is acceptable (Text S1). Fortunately the annual layer counting upon which most of the B-C core dating to 1200 CE relies is highly dependent on the insoluble dust, which is a non-diffused parameter.

The most elevated concentrations of gross beta radioactivity, reflecting concentrations of ^{137}Cs and ^{90}Sr, and concentrations of tritium (^{3}H) from atmospheric thermonuclear testing arrived in Greenland snowfall in 1963 (Koide et al., 1982; Mosley-Thompson et al., 2001) and are detected in the B-C core at ~78 m (Figure 2), in agreement with annual layer counting which has been effectively used for high accumulation (Goodwin et al., 2016) and low accumulation sites (Rasmussen et al., 2006). Six additional time-stratigraphic volcanic markers extending back to 1170 CE (Figures S1 and S2) were identified including the Tambora (Dai et al., 1991), Laki (Clausen et al., 1997), Huaynaputina (de Silva & Zielinski, 1998; Zielinski, 1995), Katla (Mosley-Thompson et al., 2001; Sigl et al., 2015), and possible local, high-latitude eruptions (Clausen et al., 1995; Fisher et al., 2004) which are discussed in more detail in the supporting information. The bottom ice may exceed 1,500 years in age (Urmann, 2009), but this has yet to be confirmed by radiometric dating, geochemical analyses, or the identification of other time-stratigraphic markers in the lowest 60 m of the core. Thus, the isotopic data discussed in this paper are restricted to those post-dating 1200 CE for which the dating uncertainty ranges from a few to a maximum of 9 years (Text S1).

2.2. Observational Data

Monthly temperature data from meteorological stations around Alaska were obtained from the Global Historical Climatology Network Version 3 (Menne et al., 2012). Eight stations around the Gulf of Alaska were chosen based on their proximity to the B-C site, and three stations were chosen further to the west (Figure 1 and Table S1). For station selection, the length and quality of their temperature records were considered. Annual average station temperatures were computed for thermal years (July–June) to coincide with annual layer delineations based on the spring dust peaks in the B-C core. Correlation coefficients were computed between annual B-C $\delta^{18}O$ and both annual and seasonal temperatures for each station. The individual station data were then averaged to create local and western Alaska temperature composites.

In the Bering Strait (Figure 1), the monthly near-bottom water temperatures from the A3 mooring are available from late-1990 to mid-2016 (Woodgate, 2018); however, several years of data are missing prior to 1998. To supplement some of these missing data, temperature measurements from the A2 mooring are used. Monthly A2 data are available from late-1990 to late-2003 (Woodgate et al., 2005). The A2 data were standardized and then recalibrated with the mean and standard deviation of the A3 data. For the 1990 to 2003 period, the A3 and recalibrated A2 data were averaged. After 2003, the mooring data are solely from A3. Correlation coefficients in this study are calculated using the combined A2/A3 mooring data. Although the magnitudes of the correlations are similar regardless of whether the A2 data are incorporated into the analysis, the statistical results are more robust given the additional degrees of freedom. Western Arctic sea ice area is determined from satellite passive-microwave data and defined as the total area across the East Siberian, Chukchi, and Bering Seas as delineated by the Goddard Space Flight Center through the National Snow and Ice Data Center (NSIDC; Fetterer et al., 2017).

2.3. Reanalysis and Modeled Data

Gridded datasets used in this study include the 20th Century Reanalysis (Compo et al., 2011) and NOAA's extended reconstructed sea surface temperatures version 4 (ERSSTv4; Huang et al., 2015, 2016; Liu et al., 2015). NOAA's Hybrid Single-Particle Lagrangian Integrated Trajectory (HYSPLIT) model (Rolph et al., 2017; Stein et al., 2015) is used to compute back trajectories from the B-C site. For the trajectory analysis, the North American Regional Reanalysis (NARR; Mesinger et al., 2006) was used for its high resolution (32 km) in this mountainous region. Two day (48 h) back trajectories were performed daily over the 1979–2001 period and were initiated at 4,700 m above sea level. Frequencies were calculated by applying a $2° \times 2°$ grid over the region and counting the number of trajectories that passed through each grid cell as a percentage of the total number of trajectories.

Isotope-enabled models have been used to further interpret paleo-proxy records of $\delta^{18}O$ from ice cores in the Andes (Hurley et al., 2016) and Greenland (Masson-Delmotte et al., 2015; Sjolte et al., 2011; Steen-Larsen et al., 2011, 2017) and proxies recovered from various locations such as the tropical Pacific (Conroy et al., 2013) and the Indian monsoon region (Midhun & Ramesh, 2016). We utilize nine simulations from six general circulation models provided by the Stable Water Isotope Intercomparison Group phase 2 project (Kurita et al., 2011; Lee et al., 2007; Risi et al., 2010, 2012; Schmidt et al., 2007; Sime et al., 2008; Yoshimura et al., 2008). Model metadata are included in Table S2. Three simulations have dynamical variables that were

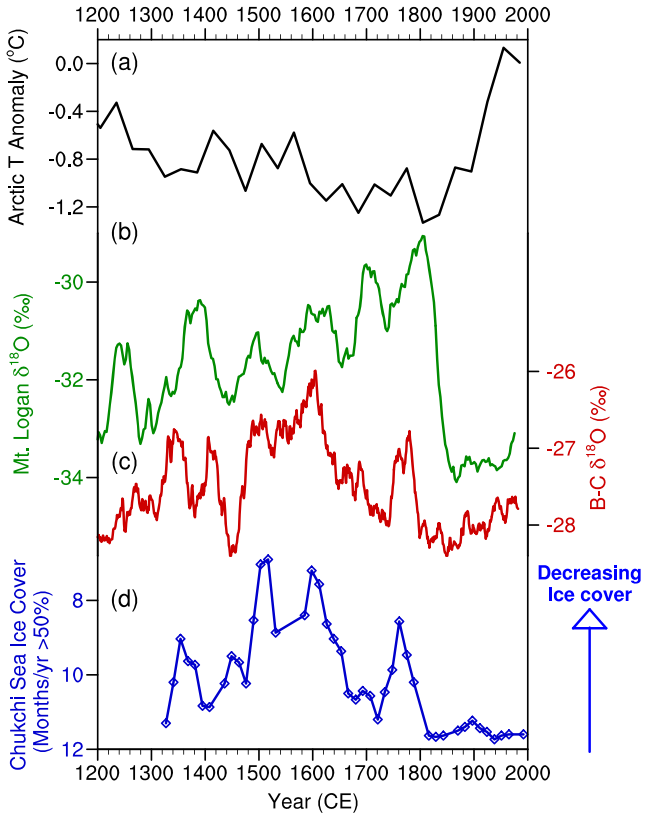

Figure 3. Time series of (a) 30-yr average Arctic-wide temperature anomalies (McKay & Kaufman, 2014), 41-yr running means of $\delta^{18}O$ on (b) Mt. Logan (Osterberg et al., 2014) and (c) B-C, and (d) Chukchi Sea ice duration as reconstructed from the 92-B5 sediment core (de Vernal et al., 2008). Note the sea ice cover axis is reversed.

adjusted or "nudged" toward reanalyses, but each model also has a free-running component. Total column ^{18}O rather than $\delta^{18}O$ of precipitation is used here for comparison with B-C $\delta^{18}O$ due to the spatial heterogeneity of precipitation in this mountainous region and the relatively low resolution of the isotope-enabled general circulation models.

3. Results

The 800-year B-C $\delta^{18}O$ record is presented here and is compared with other Arctic and North American paleoclimate proxies (Figure 3) including an Arctic-wide temperature reconstruction, the Mt. Logan ice core for which $\delta^{18}O$ data are available over the last millennium, and a high-resolution sediment core from the Chukchi Sea. Arctic-wide temperature anomalies are dominated by a gradual cooling trend from 1200 to 1800 CE, then a sharp increasing trend after 1800 CE (McKay & Kaufman, 2014; PAGES 2 k Consortium, 2013). The $\delta^{18}O$ records from Mt. Logan and B-C share almost no similarities with this Arctic-wide pattern. These differences could arise from regional variability, as many of the proxies used in the Arctic temperature reconstruction are from northeast Canada and Greenland (McKay & Kaufman, 2014). Most notably, however, neither ice core record exhibits substantial 20th century warming, which is prevalent in the Arctic-wide temperature series and is also a common trait among several tree ring-derived temperature reconstructions (Anchukaitis et al., 2013; Porter et al., 2013; Szeicz & MacDonald, 1995; Wilson et al., 2007) from northwestern North America (Figure S4), which suggests that $\delta^{18}O$ in the Mt. Logan and B-C cores is not strongly related to local temperature.

The low frequency $\delta^{18}O$ records from Mt. Logan and B-C show some interesting patterns (Figures 3b and 3c). Ostensibly, the two records appear to be very different. The most prominent feature in the Mt. Logan $\delta^{18}O$ record is the ~5‰ shift toward depleted values between 1800 and 1860 CE attributed to a switch from

local to further afield moisture sources (Fisher et al., 2004, 2008). No comparable, abrupt shift is discernible in the B-C $\delta^{18}O$ record, although both $\delta^{18}O$ records show reduced variability in the past ~150 years. Prior to 1800 CE, both ice core records show prolonged $\delta^{18}O$ enrichment during the Little Ice Age (LIA; ~1400–1850 CE), although their multidecadal scale variability is quite different. Fisher et al. (2004, 2008) concluded that Mt. Logan $\delta^{18}O$ is more enriched during the LIA because precipitation at that time originated from a local source and thus experienced less fractionation.

Although B-C $\delta^{18}O$ shows little resemblance to Arctic-wide temperatures or the neighboring Mt. Logan $\delta^{18}O$ record, the B-C data are supported by a high-resolution record of sea ice duration (de Vernal et al., 2008) from a sediment core in the Chukchi Sea (Figure 3d). The ~50-cm long marine sediment core 92-B5 was retrieved from the western Arctic in the Chukchi Sea (Figure 1) where high sedimentation rates are determined from ^{210}Pb measurements (de Vernal et al., 2008). Sea ice cover determines the amount of light penetration, and hence photosynthesis, in the upper ocean. Thus, biogenic markers, such as dinoflagellate cysts, are useful for sea ice reconstruction as their lifecycle depends on the duration of ice-free conditions. Transfer functions were used to reconstruct a ~670-year record of past sea ice duration in months per year for which sea ice concentration exceeds 50% (de Vernal et al., 2008).

The relationship between this sediment proxy record and B-C $\delta^{18}O$ over the last 670 years is remarkable ($r = -0.80$, $p < .001$), as determined by correlating the 42 discrete sediment core measurements, indicated by markers in Figure 3d, and the corresponding years in the smoothed B-C $\delta^{18}O$ record (Figure 3c). Prior to ~1500 CE, the Chukchi Sea sediment core appears to lag behind the B-C $\delta^{18}O$ record by <50 years, which likely reflects radiometric dating errors for the sediment core versus the smaller dating uncertainty for the B-C ice core dated by annual layer counting with an estimated uncertainty of 9 years or less at 1170 CE (Text S1). The sediment record and the B-C and Mt. Logan $\delta^{18}O$ records suggest that sea ice duration in the western Arctic has been relatively stable over the last 200 years.

The similarities and differences among these paleorecords raise several questions which will be explored in the following sections. First, are there physical mechanisms that can explain the close connection between B-C $\delta^{18}O$ and climate and sea ice variability in the western Arctic? Second, how might these mechanisms explain the $\delta^{18}O$ enrichment and sea ice reduction during the LIA? Third, what are some possible reasons why the $\delta^{18}O$ records from the neighboring B-C and Mt. Logan drill sites are so different?

3.1. Physical Mechanisms Linking the B-C Site to the Western Arctic

The dissimilarities between B-C $\delta^{18}O$ and temperature reconstructions from tree rings around northwestern North America (Figure S4) suggest that B-C $\delta^{18}O$ does not reflect local temperature. To further investigate the relationship between $\delta^{18}O$ and temperature, meteorological station data (Figure 1 and Table S1) have been composited into local and western Alaska temperature series and correlated with B-C $\delta^{18}O$ (correlations with individual station temperatures are given in Table S3). B-C $\delta^{18}O$ shows little coherence with the local meteorological station annual temperature composite (Figure 4a). Correlations between annual B-C $\delta^{18}O$ and local seasonal temperature composites are given in Table S4, and the coefficients are generally weak and/or negative. These stations are relatively low elevation (Table S1) compared to the B-C site, which may explain some of the disparity. However, B-C $\delta^{18}O$ is more similar to station temperatures composited across western Alaska during the spring season (Figure 4b and Table S5). For the western station composite, seasonal correlations with B-C $\delta^{18}O$ were strongest in the spring (AMJ) and summer (JAS; Table S5). The correlation between the AMJ western temperature composite and B-C $\delta^{18}O$ is somewhat low ($r = 0.27$, $p = .01$), however, this coefficient increases considerably after 1950 ($r = 0.45$; Table S5). This is explained by the divergence at ~1940 CE when temperatures were well above average due to a strong, prolonged El Niño event (Brönniman et al., 2004) and B-C $\delta^{18}O$ was substantially depleted (Figure 4b). When the few years around this event (1935–1945) are removed from the analysis, the correlation coefficient increases to 0.50. Thus, the relationships among the B-C $\delta^{18}O$ record and meteorological station temperatures reveal a climatic connection between the B-C site and western Alaska. This connection appears strongest in spring when the primary storm track is shifting northward toward the Bering Sea, which may serve as an additional moisture source region.

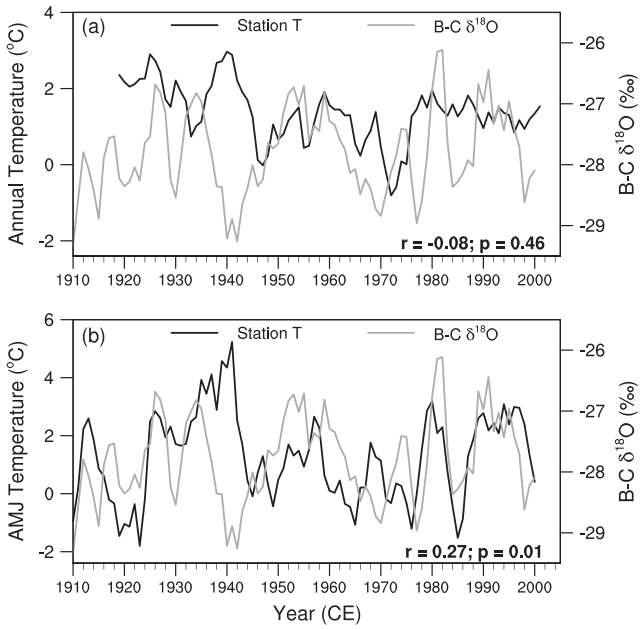

Figure 4. 3-yr running means of annual average B-C $\delta^{18}O$ (gray) and the (a) local and (b) western station temperature composites (black). Note the western station temperature composite is for spring (AMJ). Correlation coefficients for individual stations and the remaining seasons are included in Tables S3–S5.

Back trajectories with NOAA's HYSPLIT model were determined for the B-C site to further explore possible moisture source regions. Without automatic weather station data at the B-C site, it is difficult to ascertain the precise timing of precipitation events. Thus, trajectories are constrained to both precipitating and nonprecipitating air masses. Trajectory frequencies tend to show air masses approaching the B-C site from the Gulf of Alaska (not shown). To determine how different trajectories influence the isotopic record, we delineate trajectories based on years of high and low B-C $\delta^{18}O$. Figure 5 shows the difference in the spring trajectory frequencies between the five most isotopically enriched and five most isotopically depleted years in the B-C core. Air masses approaching from the west and southwest are enriched in $\delta^{18}O$ while air masses from the south and southeast are depleted. The other seasons exhibit a similar pattern of enriched $\delta^{18}O$ air masses from the west and/or southwest with the exception of autumn (OND) where this pattern is reversed (Figure S5). Fisher et al. (2004) argue that enriched $\delta^{18}O$ on Mt. Logan occurs when moisture originates from more local, rather than distant, sources and is associated with zonal flow. Observations discussed by Bailey et al. (2019) indicate that $\delta^{18}O$ in precipitation over Anchorage is enriched when storms approach from the west and southwest due to fewer topographical barriers and associated rainout. Storms more commonly approach from the west during the spring season (Bailey et al., 2019), which partially explains why western station temperatures were most strongly correlated to B-C $\delta^{18}O$ during spring (Figure 4b and Table S5). Isotopes at B-C are similarly enriched when storms approach from the west or southwest, but whether this is explained by the original moisture source characteristics, topography, or a combination of these factors has yet to be determined.

The location and intensity of the North Pacific storm track is characterized by the Aleutian Low. A stronger Aleutian Low shifts slightly eastward and is accompanied by strong southerly flow of warm, moist air into the Gulf of Alaska and northerly flow over the Bering Sea on the backside of the Low (Rodionov et al., 2007). The warm, moist air flowing into the Gulf of Alaska transports enriched isotopes into the region according to $\delta^{18}O$ precipitation observations (Bailey et al., 2015) and model results (Field et al., 2010). A weaker Aleutian Low often shifts westward directing storms into the Bering Sea, but may also split into two low pressure centers, one near Kamchatka and the other in the Gulf of Alaska (Rodionov et al., 2007). The strength and position of the Aleutian Low have been shown to influence temperature and precipitation in Alaska (Mock et al., 1998). Several large-scale climate oscillations that influence or describe the strength of the Aleutian Low include the Pacific Decadal Oscillation, North Pacific Index, Pacific-North American

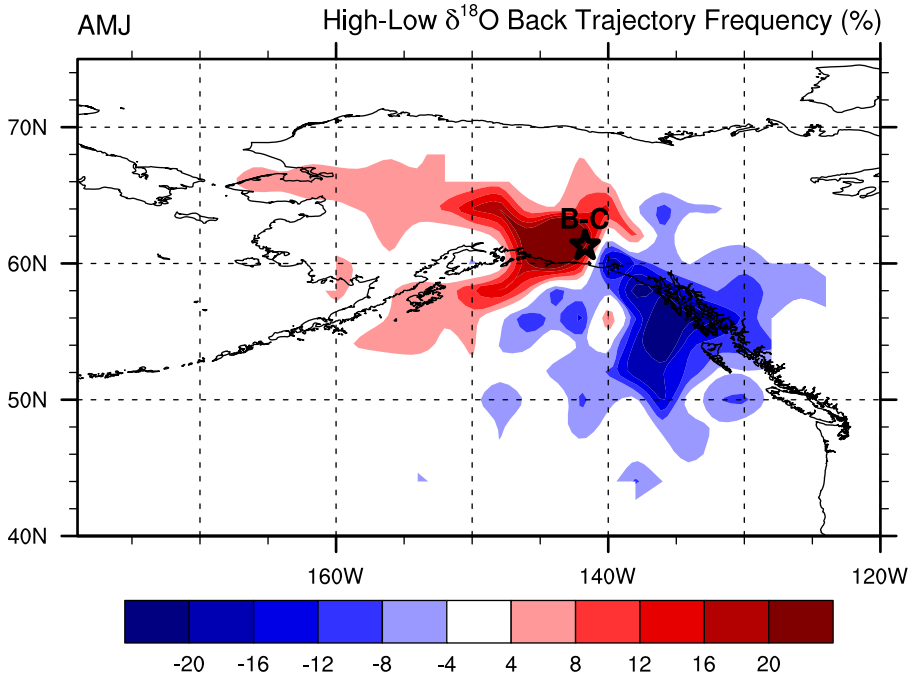

Figure 5. The difference in spring (AMJ) back trajectory frequencies between the five most enriched (highest) and five most depleted (lowest) years of B-C $\delta^{18}O$ for the 1979-2001 CE period. Results for each season are provided in the supporting information (Figure S5).

pattern, and Arctic Oscillation. B-C $\delta^{18}O$ is not significantly correlated to any of these indices; thus its direct connection with the Aleutian Low strength is difficult to ascertain, especially as paleo-indicators of Aleutian Low strength are contradictory (Bailey et al., 2015; Kaufman et al., 2016).

During spring, B-C $\delta^{18}O$ is related to meridional flow over the Bering Sea and the Gulf of Alaska (Figure 6a), although the relationships are reversed. Southerly flow over the Bering Sea (Gulf of Alaska) coincides with enriched (depleted) $\delta^{18}O$ at the B-C site. This pattern is apparent in the annual signal but is strongest in winter and spring (Figure S6). Enriched B-C $\delta^{18}O$ also coincides with higher springtime sea surface temperatures (SSTs) through the Bering Strait (Figure 6b) and lower SSTs in the Gulf of Alaska. These two features, although correlatively weak, are discernible among the seasons (Figure S7). The inflow of warm air and water to the Bering Sea in spring strongly influences the onset of seasonal sea ice retreat (Serreze et al., 2016; Woodgate et al., 2010). This is demonstrated by near-bottom water temperatures in the Bering Strait, as measured by the A2 and A3 moorings (Woodgate, 2018), which are most strongly related to western Arctic sea ice area in spring (AMJ; $r = -0.725$, $p < .001$; Figure 6c and Table S6) when sea ice decays.

Enriched B-C $\delta^{18}O$ coincides with reduced sea ice area in the western Arctic (Figure 6d; $r = -0.458$, $p = .028$) that accompanies enhanced springtime meridional flow in the Bering Sea. This relationship is only significant in spring (Table S6). Thus, enriched B-C $\delta^{18}O$ reflects warmer waters in the Bering Strait and reduced sea ice area throughout the western Arctic. Woodgate (2018) reports that annual mooring temperatures sharply increase after 2001, which coincides with an accelerating decline in late summer/early autumn sea ice area in the western Arctic due to warming waters in the western and central North Pacific, enhanced poleward moisture transport, and resulting feedback mechanisms (Lee et al., 2017). Springtime sea ice extent may also be declining more quickly as evidenced by the notably low extent in the Bering Sea during the 2018 and 2019 seasons (NSIDC, 2019).

Observational evidence from meteorological stations, Bering Strait moorings, and satellites suggests that the connection between B-C $\delta^{18}O$ and the western Arctic climate is strongest in spring. This is a surprising finding as storm tracks tend to be strongest in winter and stations in the Alaska interior near the B-C site receive the bulk of their precipitation in summer (Bieniek et al., 2012). Recent studies have focused on the

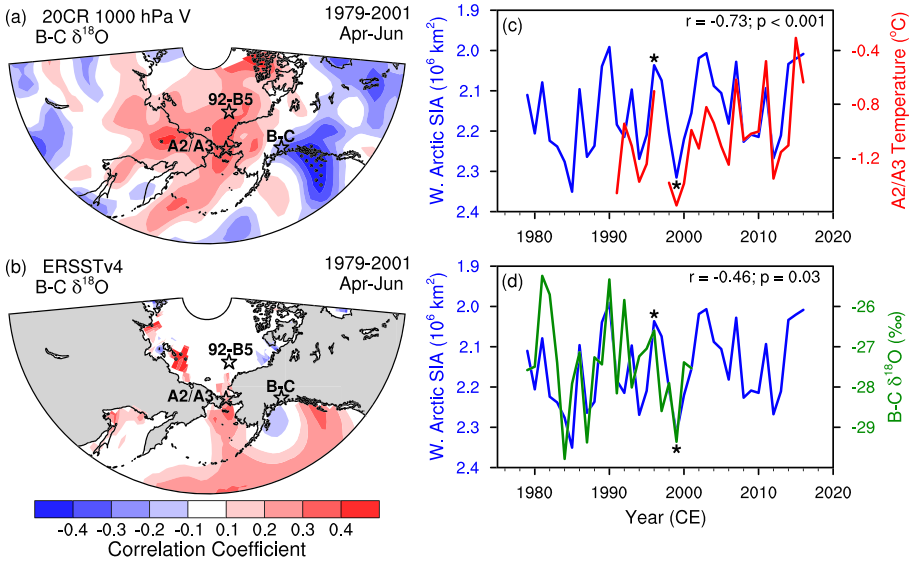

Figure 6. Spatial correlations between B-C $\delta^{18}O$ and (a) 1000 hPa meridional wind (V) from 20th Century Reanalysis (Compo et al., 2011) and (b) SSTs from NOAA's extended reconstructed sea surface temperatures (Huang et al., 2015, 2016; Liu et al., 2015) for spring (AMJ) 1979–2001 CE. Stippling indicates 95% significance. Stars indicate the B-C site, A2/A3 moorings, and sediment core (92-B5) location. Correlations for the other seasons are provided in the supporting information (Figures S6 and S7). (c,d) Time series of AMJ western Arctic sea ice area (blue), AMJ A2 and A3 mooring temperatures (red; Woodgate, 2018), and annual B-C $\delta^{18}O$ (green). Note that the sea ice area axis is inverted. Asterisks denote the warm (1996) and cold (1999) scenarios discussed in the text.

springtime dynamics in the western Arctic, including the influence of the Aleutian Low on Bering Strait inflow and Alaska snowmelt (Cox et al., 2019) and the influence of clouds on sea ice extent (Huang et al., 2019). Focusing on two of the extremes, the spring of 1996 demonstrates a warm scenario wherein B-C $\delta^{18}O$ is enriched, sea ice area is reduced, and Bering Strait waters are warmer; while the spring of 1999 represents the colder counterpart (asterisks in Figures 6c and 6d). The 1996 temperature anomalies from the preceding winter (Figure S8a) indicate a scenario reminiscent of the warm Arctic/cold continents pattern which typically accompanies reduced sea ice in the Arctic (Cohen et al., 2013; Overland et al., 2011). Cohen et al. (2012) determined that warmer Arctic summers and reduced Arctic sea ice increase moisture availability and hence snow cover over Eurasia. This increase in snow cover can weaken the polar vortex thereby initiating cold air outbreaks over the mid-latitudes. A northwesterly displaced storm track would likely accompany this pattern, suggesting that more storms from the west would influence the B-C site, thereby enriching $\delta^{18}O$. The temperature anomalies for the winter of 1999 (Figure S8b) indicate warmer continents, especially North America and Europe, while the western Arctic is colder than average. Thus, climate signals recorded in the B-C ice core may not be consistent with other Northern Hemisphere continental records as these signals would vary depending on the trough-ridge structure of atmospheric waves.

3.2. Reduction of Sea Ice Duration and $\delta^{18}O$ Enrichment During much of the LIA

According to 20th century observations, B-C $\delta^{18}O$ is linked to western Arctic sea ice through changes in the storm track and resulting inflow through the Bering Strait. Enriched $\delta^{18}O$ at B-C and Mt. Logan and reduced sea ice duration are evident from 1400 to 1850 CE (i.e., the LIA; Figure 3). Assuming these relationships are stationary over the paleorecord, then, the enriched $\delta^{18}O$ and reduced sea ice cover during much of the LIA suggest a northward shifted storm track and increased southerly flow in the Bering Sea. With reduced sea ice in the Bering Sea, the storm track likely shifted northwestward to follow the margin of baroclinicity as reduced arctic sea ice is associated with weaker westerlies and less intense storms north of 45°N (Budikova, 2009). Likewise, Arctic amplification has been speculatively linked to reduced westerly winds as the temperature gradient between the Arctic and mid-latitudes weakens (Francis & Vavrus, 2012). This would likely result in a weaker storm track, possibly shifting northward as is typical during the winter to spring transition.

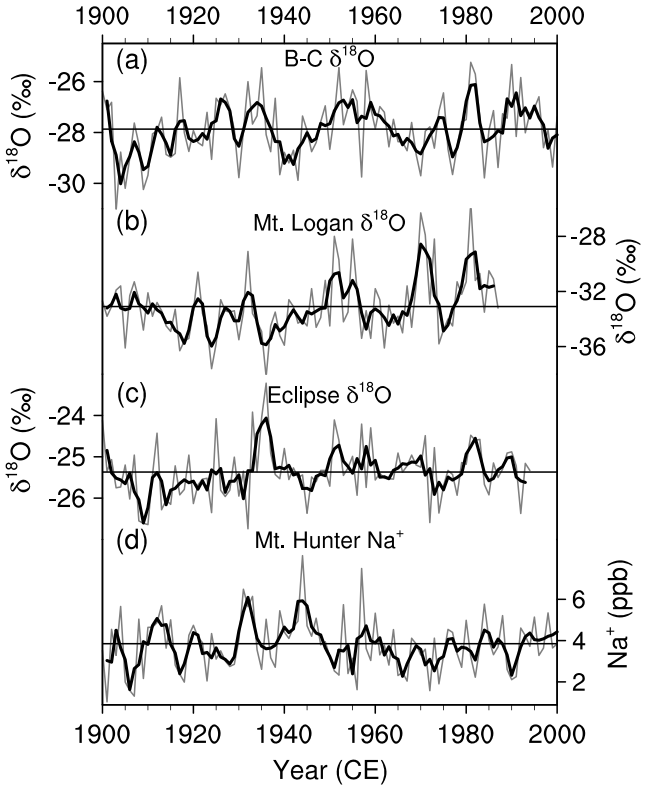

Figure 7. Twentieth century ice core $\delta^{18}O$ records from northwestern North America. Average $\delta^{18}O$ from (a) B-C, (b) Mt. Logan (Holdsworth et al., 1992; Moore, Holdsworth, et al., 2002), and (c) Eclipse ice core (Wake et al., 2002), and Na^+ from (d) Mt. Hunter ice core (Osterberg et al., 2017). No isotope data are available from the Mt. Hunter core as of the date of submission. Annual averages (gray) and 3-yr running means (black) are shown.

On larger spatial scales, LIA climate signatures are not particularly synchronous or uniform (Jones & Mann, 2004). Yet, reduced sea ice cover and warmer conditions during the LIA have been observed Arctic-wide (Kinnard et al., 2011), in the Fram Strait (Bonnet et al., 2010), in Baffin Bay (Hughen et al., 2000), and over the Beaufort Sea (Richerol et al., 2008), although the timing varies slightly among these proxies. Modeling studies also indicate warmer conditions in the North Pacific (Shindell et al., 2001). This Arctic warmth during the LIA could indicate a prolonged period of the warm Arctic/cold continents pattern (Cohen et al., 2013; Overland et al., 2011) as was observed in the winter of 1996 CE (Figure S8a), which preceded warmer spring conditions in the western Arctic. A prolonged warm Arctic/cold continents pattern would create colder conditions over much of North America and Europe where paleorecords exhibit a more well-defined LIA cold period (Jones & Mann, 2004; Shindell et al., 2001). Thus, the dissimilarity between the warmer LIA in the western Arctic records and colder LIA evident in northern mid-latitude records likely depends on the prevailing trough-ridge structure of atmospheric waves.

Temperature reconstructions from tree ring records in this region generally indicate cooler LIA conditions with only brief warm excursions during the 16th and late 18th centuries (Figure S4). Glacier advances also occurred in southern Alaska due to lower summer temperatures during the LIA (Barclay et al., 1999; Davi et al., 2003; Wiles et al., 2004). A northwardly displaced storm track would increase storms through the Bering Sea and decrease storm frequency in the Gulf of Alaska. Storms entering the Gulf of Alaska and southern Alaska bring warm, maritime air to the region, thus if these storms were less frequent, colder and drier conditions would be expected in southern Alaska. A northward shift in the storm track is supported by lake records in the Alaskan interior which show increased moisture availability for Farewell Lake (Hu et al., 2001) in the western interior and lower lake levels at Grizzly Lake (Tinner et al., 2008) in the southeastern interior. Colder and wetter conditions in the Alaskan interior are also linked to westerly flow across the Bering Sea (Mock et al., 1998), which would be expected with a weaker Aleutian Low. This resulting zonal flow would enrich $\delta^{18}O$ in the snow on B-C and Mt. Logan.

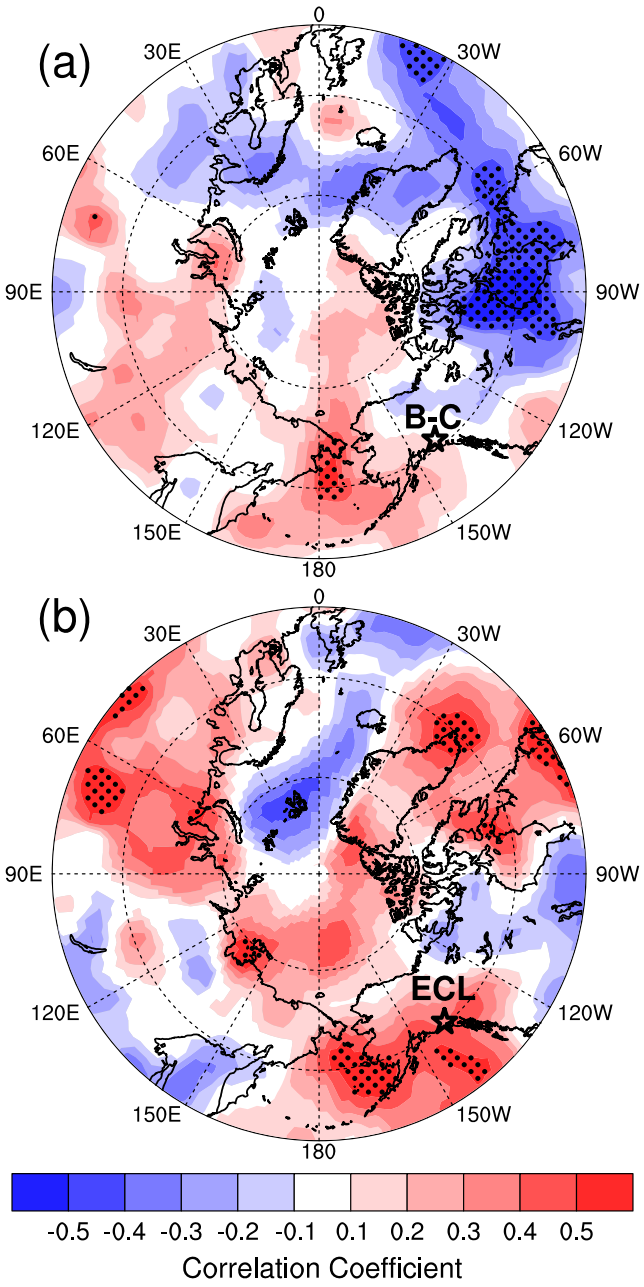

Figure 8. Spring (AMJ) total column ^{18}O from the nudged isotope-enabled General Spectral Model (IsoGSM; Yoshimura et al., 2008) is correlated with annual (a) B-C $\delta^{18}O$ for the 1979–2001 period and (b) Eclipse (ECL) $\delta^{18}O$ for the 1979–1994 period. Stippling indicates 95% significance. Results for each season and for each model are provided in the supporting information (Figures S9-S11).

The LIA enrichment of $\delta^{18}O$ in both the B-C and Mt. Logan cores may also reflect changes in the seasonality of precipitation. Over the latter half of the 20th century, both southeastern and western Alaska have experienced increasing temperatures and increasing (decreasing) winter (summer) precipitation (Bieniek et al., 2014; Stafford et al., 2000). Thus, assuming that this relationship is linear and persistent, decreasing continental temperatures, such as those during the LIA, would be associated with enhanced summer and reduced winter precipitation, thereby biasing the annual average ice core–derived $\delta^{18}O$ record toward the summer season (enriched $\delta^{18}O$). LIA characteristics of the B-C accumulation record will be explored in future work.

3.3. Dissimilarity Among Ice Core–Derived Climate Histories in This Region

Although $\delta^{18}O$ records from the B-C and Mt. Logan ice cores show some similarities such as LIA enrichment and reduced variability in the recent ~150 years, the records are otherwise quite different (Figure 3). The complex topography of this region creates a large degree of spatial heterogeneity among local climate parameters. Here $\delta^{18}O$ strongly depends on elevation which determines local versus regional moisture sources and the degree of isotopic fractionation (Fisher et al., 2004; Holdsworth et al., 1991). Several ice cores have been retrieved from varying elevations in the Wrangell-St. Elias mountain range, and the B-C site is situated at an intermediate elevation between the Mt. Logan and Eclipse ice core sites. The B-C $\delta^{18}O$ record is compared with their $\delta^{18}O$ records to determine the degree of spatial heterogeneity among these records. (Figure 7 and Table S7). The interannual $\delta^{18}O$ variability increases with altitude such that Mt. Logan, B-C, and Eclipse exhibit standard deviations of 2.3‰, 1.2‰, and 0.66‰, respectively. Only Mt. Logan shows a significant increasing trend (0.27‰ per decade; $p = .005$) over the 20th century. B-C $\delta^{18}O$ is weakly correlated with both Eclipse $\delta^{18}O$ ($r = 0.21$, $p = .04$) and Mt. Logan $\delta^{18}O$ ($r = 0.20$, $p = .07$). Likewise, given that $\delta^{18}O$ indicates different climate parameters for Mt. Logan (i.e., moisture source) and Eclipse (i.e., local temperature), these cores are also very weakly correlated ($r = 0.09$, $p = 0.39$) over the 20th century. Thus, despite their regional proximity, these three ice core $\delta^{18}O$ records exhibit noticeable dissimilarities over the 20th century likely due to differences in their specific location, elevation, and orientation in the complex mountainous terrain.

For the 20th century, a weak negative correlation exists between B-C $\delta^{18}O$ and Na^+ from the Mt. Hunter ice core from the interior Alaska Range ($r = -0.21$, $p = .04$; Table S7) such that isotopically depleted periods on B-C generally correspond to periods of higher sodium (Na^+) concentrations in the Mt. Hunter core (for which $\delta^{18}O$ data are not yet available). Higher Na^+ concentrations on Mt. Hunter are associated with a stronger Aleutian Low (Osterberg et al., 2017), which suggests that B-C $\delta^{18}O$ depletion is also associated with a stronger Aleutian Low. This is similar to the Mt. Logan core which exhibits depleted isotopes when the Aleutian Low is strong, thereby increasing southerly advection and tapping moisture sources that are further afield (Fisher et al., 2004, 2008). If this were also the case for the B-C core, one would expect the $\delta^{18}O$ records from B-C and Mt. Logan to exhibit more coherence, yet they are quite different (Figure 7). Furthermore, Mt. Logan $\delta^{18}O$ has experienced an increasing trend over the latter part of the 20th century (0.35‰ per decade since 1950; Figure 7) over the same period when the Aleutian Low has been deepening (Gan et al., 2017).

The B-C site is situated further inland than Mt. Logan and just north of the split between the Wrangell-Saint Elias and Chugach mountain ranges (Figure 1). Thus, the orographic effect likely has a stronger influence on the B-C site than on Mt. Logan. Storms from the west and southwest may be less subject to the coastal orography thereby enriching B-C $\delta^{18}O$, and storms may preferentially traverse topographic lows such as the Cook Inlet and other prominent river valleys (Bailey et al., 2019; Lachniet et al., 2016). Without automatic weather station data or high-resolution models capable of accurately capturing the complex terrain, it is uncertain how an individual storm system would uniquely affect each site in this region.

Simulations from isotope-enabled general circulation models (Table S2) were used to elucidate some of the differences between the B-C ice core and the neighboring Eclipse ice core. The Mt. Logan $\delta^{18}O$ data end in 1987 which provides less than 10 years of overlap with the isotope-enabled models, many of which only date back to 1979; thus, Mt. Logan was excluded from this analysis. Although we use the total column ^{18}O rather than precipitated ^{18}O as discussed in section 2.3, the models simulate ^{18}O at the B-C site modestly well and even significantly so when using a subset ensemble ($r = 0.46$, $p = .03$; Table S8). Results from the nudged models show that the connection between B-C $\delta^{18}O$ and the Bering Sea is strongest in spring (Figure S9), similar to the relationships observed with station temperatures in western Alaska (Figure 4b and Table S5) and western Arctic sea ice (Figure 6 and Table S6). In summer (JAS) when atmospheric circulation is generally weaker, correlations are strongly positive over the Gulf of Alaska, suggesting a more local influence (Figure S9). Focusing on spring, the nudged isotope-enabled General Spectral Model (IsoGSM; Yoshimura et al., 2008) indicates that B-C $\delta^{18}O$ shows a more isolated signal over the Bering Sea while Eclipse $\delta^{18}O$ shows connections with both the Bering Sea and the Gulf of Alaska (Figure 8). Thus, it is possible that the receipt of moisture from both source regions partially masks the signal of Bering Sea climate variability in the Eclipse $\delta^{18}O$ record. For the B-C site, most of the isotope-enabled models show very little influence from the Gulf of Alaska (Figure S10) which may partially explain why the B-C $\delta^{18}O$ record exhibits little commonality with the $\delta^{18}O$ records from the other two ice cores. Despite a large spread, the suite of models generally

suggests that the Bering Sea may serve as a moisture source for both the B-C and Eclipse sites (Figures S10 and S11) during spring; however, the input signal from the Bering Sea should be much clearer on B-C than on Eclipse which is additionally influenced by the Gulf of Alaska, in agreement with previous results (Fisher et al., 2004; Kelsey et al., 2012), and possibly other further afield sources.

Isotope-enabled models, reanalysis data, and observations all demonstrate the connection between the Bering Sea climate and B-C $\delta^{18}O$. Furthermore, while some isotope-enabled model simulations are nudged to reanalysis data, the dynamics in a free-running (i.e., unnudged) model (Yoshimura et al., 2008) provide additional support for this relationship such that modeled total column ^{18}O over the B-C drill site is influenced by meridional winds over the Bering Sea during the spring season (Figure S12). These modeled correlations indicate that the transport mechanisms in the model linking the Bering Sea ^{18}O to the B-C site are similar to those observed. Thus, based on post-1979 observations, the B-C $\delta^{18}O$ record demonstrates strong potential to provide additional insight to western Arctic climate and sea ice variability prior to the advent of satellite records.

4. Conclusions

The Arctic is experiencing rapid climatic and environmental changes with the potential to influence mid-latitude weather, and hence the climate. Several high-resolution paleorecords (e.g., tree rings and ice cores) are available from northwestern North America to better define the regional climate history and contextualize the 20th century changes. Stable oxygen isotopes, usually a temperature proxy, from the B-C ice core are only weakly related to local temperature, but show a stronger connection to station temperatures across western Alaska. Isotope-enabled models also demonstrate that B-C $\delta^{18}O$ is correlated with the atmospheric ^{18}O over the Bering Sea, primarily in the spring season. Reanalysis data and various observations including sea ice cover, meteorological station temperatures, and Bering Strait mooring data indicate that B-C $\delta^{18}O$ is related to the meridional air flow and ocean temperatures primarily over the Bering Sea, and also confirm that this connection is stronger in the spring. Furthermore, back trajectory analysis indicates that air masses with enriched $\delta^{18}O$ typically approach B-C from the west and southwest, while air masses depleted in $\delta^{18}O$ approach from the south and southeast. Whether these depleted air masses originate from further afield sources or result from a stronger orographic effect remains uncertain. We posit that the microclimate induced by location, elevation, and orientation in this complex mountainous terrain plays a larger role given the noticeable dissimilarities among ice core $\delta^{18}O$ records from this region over the 20th century. Nevertheless, multiple lines of evidence suggest that B-C $\delta^{18}O$ is linked with the western Arctic climate, and that variability in the meridional flow and water temperature in the Bering Sea influences the heat flux into the Arctic, which in turn affects sea ice cover in the western Arctic.

The high resolution B-C $\delta^{18}O$ record provides a rare and valuable history of climate variability in the western Arctic and especially of sea ice cover over the last millennium. Its veracity is supported by a 670-year record of sea ice cover extracted from a marine sediment core in the Chukchi Sea. A prominent feature of the B-C $\delta^{18}O$ record is the enriched $\delta^{18}O$ from ~1400 to 1850 CE, contemporaneous with much of the LIA, which suggests warmer conditions and reduced sea ice cover in the western Arctic. This may be related to the warm Arctic/cold continents pattern which initiates cold air outbreaks over the mid-latitudes when the polar vortex weakens under warmer Arctic conditions. A northwesterly displaced storm track would likely accompany this pattern suggesting that more storms from the west would influence the B-C site, thereby enriching $\delta^{18}O$. Seasonality of precipitation may also play a role in this LIA enrichment of B-C $\delta^{18}O$. Overall, the 800-year B-C $\delta^{18}O$ record provides a high-resolution history of climate variability and sea ice cover in the western Arctic region. The remaining ~60 m of the B-C core have been analyzed for $\delta^{18}O$, and when a robust time scale is established, these data should offer the potential for an even longer record of regional sea ice cover.

Acknowledgments
The authors wish to thank two anonymous reviewers for their comments and suggestions which greatly improved the clarity and organization of the manuscript. The authors thank the members of The Ohio State University (OSU) drill team who collected the Bona-Churchill ice core (Lonnie Thompson, team leader, Victor Zagorodnov, Vladimir Mikhalenko, Keith Mountain, David Urmann, Patrick Ginot, John Paskievitch, Mary Davis, Tracy Mashiotta, and Amanda Cavin). Mary Davis analyzed the dust content and ionic concentrations, Pingnan Lin analyzed the stable water isotopes, and Lonnie Thompson and David Urmann constructed the timescale. The project was funded by the NSF-OPP-0099311 award to Lonnie Thompson and Ellen Mosley-Thompson. 20CR and ERSSTv4 data were provided by NOAA/OAR/ESRL Physical Sciences Division in Boulder, CO (https://www.esrl.noaa.gov/psd/). NOAA's HYSPLIT model was provided by the NOAA Air Resources Laboratory (http://www.ready.noaa.gov). SWING2 simulations were obtained from https://data.giss.nasa.gov/swing2/. Data from this study are available at https://www.ncdc.noaa.gov/paleo-search/study/27810. This is Byrd Polar and Climate Research Center contribution number 1570.

References

Anchukaitis, K. J., D'Arrigo, R. D., Andreu-Hayles, L., Frank, D., Verstege, A., Curtis, A., et al. (2013). Tree-ring reconstructed summer temperatures from northwestern North America during the last nine centuries. *Journal of Climate*, *26*(10), 3001–3012. https://doi.org/10.1175/JCLI-D-11-00139.1

Bailey, H. L., Kaufman, D. S., Henderson, A. C. G., & Leng, M. J. (2015). Synoptic scale controls on the $\delta^{18}O$ in precipitation across Beringia. *Geophysical Research Letters*, *42*, 4608–4616. https://doi.org/10.1002/2015GL063983

Bailey, H. L., Klein, E. S., & Welker, J. M. (2019). Synoptic and mesoscale mechanisms drive winter precipitation $\delta^{18}O/\delta^{2}H$ in south-central Alaska. *Journal of Geophysical Research: Atmospheres*, *124*, 4252–4266. https://doi.org/10.1029/2018JD030050

Barclay, D. J., Wiles, G. C., & Calkin, P. E. (1999). A 1119-year tree-ring-width chronology from western Prince William Sound, southern Alaska. *Holocene*, *9*(1), 79–84. https://doi.org/10.1191/095968399672825976

Bieniek, P. A., Bhatt, U. S., Rundquist, L. A., Lindsey, S. D., Zhang, X., & Thoman, R. L. (2011). Large-scale climate controls of interior Alaska river ice breakup. *Journal of Climate*, *24*(1), 286–297. https://doi.org/10.1175/2010JCLI3809.1

Bieniek, P. A., Bhatt, U. S., Thoman, R. L., Angeloff, H., Partain, J., Papineau, J., et al. (2012). Climate divisions for Alaska based on objective methods. *Journal of Applied Meteorology and Climatology*, *51*(7), 1276–1289. https://doi.org/10.1175/JAMC-D-11-0168.1

Bieniek, P. A., Walsh, J. E., Thoman, R. L., & Bhatt, U. S. (2014). Using climate divisions to analyze variations and trends in Alaska temperature and precipitation. *Journal of Climate*, *27*(8), 2800–2818. https://doi.org/10.1175/JCLI-D-13-00342.1

Bonnet, S., de Vernal, A., Hillaire-Marcel, C., Radi, T., & Husum, K. (2010). Variability of sea-surface temperature and sea-ice cover in the Fram Strait over the last two millennia. *Marine Micropaleontology*, *74*(3-4), 59–74. https://doi.org/10.1016/j.marmicro.2009.12.001

Brönniman, S., Luterbacher, J., Staehelin, J., Svendby, T. M., Hansen, G., & Svenøe, T. (2004). Extreme climate of the global troposphere and stratosphere in 1940-42 related to El Niño. *Nature*, *431*(7011), 971–974. https://doi.org/10.1038/nature02982

Budikova, D. (2009). Role of Arctic sea ice in global atmospheric circulation: A review. *Global and Planetary Change*, *68*(3), 149–163. https://doi.org/10.1016/j.gloplacha.2009.04.001

Clausen, H. B., Hammer, C. U., Christensen, J., Schøtt Hvidberg, C., Dahl-Jensen, D., Legrand, M., & Steffensen, J. P. (1995). 1250 years of global volcanism as revealed by Central Greenland ice cores. In R. J. Delmas (Ed.), *Ice Core Studies of Global Biogeochemical Cycles*, (pp. 175–194). Berlin: Springer.

Clausen, H. B., Hammer, C. U., Hvidberg, C. S., Dahl-Jensen, D., Steffensen, J. P., Kipfstuhl, J., & Legrand, M. (1997). A comparison of the volcanic records over the past 4000 years from the Greenland Ice Core Project and Dye 3 Greenland ice cores. *Journal of Geophysical Research*, *102*(C12), 26707–26723. https://doi.org/10.1029/97JC00587

Cohen, J., Jones, J., Furtado, J. C., & Tziperman, E. (2013). Warm Arctic, cold continents: A common pattern related to Arctic sea ice melt, snow advance, and extreme winter weather. *Oceanography*, *26*(4), 150–160. https://doi.org/10.5670/oceanog.2013.70

Cohen, J. L., Furtado, J. C., Barlow, M. A., Alexeev, V. A., & Cherry, J. E. (2012). Arctic warming, increasing snow cover and widespread boreal winter cooling. *Environmental Research Letters*, *7*(1), 014007. https://doi.org/10.1088/1748-9326/7/1/014007

Compo, G. P., Whitaker, J. S., Sardeshmukh, P. D., Matsui, N., Allan, R. J., Yin, X., et al. (2011). The Twentieth Century Reanalysis Project. *Quarterly Journal of the Royal Meteorological Society*, *137*(654), 1–28. https://doi.org/10.1002/qj.776

Conroy, J. L., Cobb, K. M., & Noone, D. (2013). Comparison of precipitation isotope variability across the tropical Pacific in observations and SWING2 model simulations. *Journal of Geophysical Research: Atmospheres*, *118*, 5867–5892. https://doi.org/10.1002/jgrd.50412

Cox, C. J., Stone, R. S., Douglas, D. C., Stanitski, D. M., & Gallagher, M. R. (2019). The Aleutian Low-Beaufort Sea Anticyclone: A climate index correlated with the timing of springtime melt in the Pacific Arctic cryosphere. *Geophysical Research Letters*, *46*, 7464–7473. https://doi.org/10.1029/2019GL083306

Cuffey, K. M., & Paterson, W. S. B. (2010). *The physics of glaciers*. Amsterdam: Elsevier.

Dai, J., Mosley-Thompson, E., & Thompson, L. G. (1991). Ice core evidence for an explosive tropical volcanic eruption 6 years prior to Tambora. *Journal of Geophysical Research*, *96*(D9), 17361–17366. https://doi.org/10.1029/91JD01634

Dansgaard, W. (1954). The O^{18}-abundance in fresh water. *Geochimica et Cosmochimica Acta*, *6*(5-6), 241–260. https://doi.org/10.1016/0016-7037(54)90003-4

Dansgaard, W. (1964). Stable isotopes in precipitation. *Tellus*, *16*(4), 436–468. https://doi.org/10.3402/tellusa.v16i4.8993

Davi, N. K., Jacoby, G. C., & Wiles, G. C. (2003). Boreal temperature variability inferred from maximum latewood density and tree-ring width data, Wrangell Mountain region, Alaska. *Quaternary Research*, *60*(3), 252–262. https://doi.org/10.1016/j.yqres.2003.07.002

de Silva, S. L., & Zielinski, G. A. (1998). Global influence of the AD 1600 eruption of Huaynaputina, Peru. *Nature*, *393*(6684), 455–458. https://doi.org/10.1038/30948

de Vernal, A., Hillaire-Marcel, C., Solignac, S., & Radi, T. (2008). Reconstructing sea ice conditions in the Arctic and sub-Arctic prior to human observations. In E. T. DeWeaver, C. M. Bitz, & L. B. Tremblay (Eds.), *Arctic Sea Ice Decline: Observations, Projections, Mechanisms, and Implications, Geophysical Monograph Series*, (Vol. 180, pp. 27–45). Washington, DC: American Geophysical Union.

Dethloff, K., Rinke, A., Benkel, A., Koltzow, M., Sokolova, E., Kumar Saha, S., et al. (2006). A dynamical link between the Arctic and the global climate system. *Geophysical Research Letters*, *33*, L03703. https://doi.org/10.1029/2005GL025245

Fetterer, F., Knowles, K., Meier, W., Savoie, M., & Windnagel, A. K. (2017). Sea Ice Index, Version 3 National Sea Ice Data Center. Available at https://doi.org/10.7265/N5K072F8. Accessed October 26, 2017.

Field, R. D., Moore, G. W. K., Holdsworth, G., & Schmidt, G. A. (2010). A GCM-based analysis of circulation controls on $\delta^{18}O$ in the southwest Yukon, Canada: Implications for climate reconstructions in the region. *Geophysical Research Letters*, *37*, L05706. https://doi.org/10.1029/2009GL041408

Fisher, D. A., Osterberg, E., Dyke, A., Dahl-Jensen, D., Demuth, M., Zdanowicz, C., et al. (2008). The Mt Logan Holocene-late Wisconsinan isotope record: tropical Pacific-Yukon connections. *The Holocene*, *18*(5), 667–677. https://doi.org/10.1177/0959683608092236

Fisher, D. A., Wake, C., Kreutz, K., Yalcin, K., Steig, E., Mayewski, P., et al. (2004). Stable isotope records from Mount Logan, Eclipse ice cores and nearby Jellybean Lake. Water cycle of the North Pacific over 2000 years and over five vertical kilometres: sudden shifts and tropical connections. *Géographie Physique et Quaternaire*, *58*(2-3), 337–352. https://doi.org/10.7202/013147ar

Fleming, M. D., Chapin, F. S. III, Cramer, W., Hufford, G., & Serreze, M. (2000). Geographic patterns and dynamics of Alaskan climate interpolated from a sparse station record. *Global Change Biology*, *6*(S1), 49–58. https://doi.org/10.1046/j.1365-2486.2000.06008.x

Francis, J. A., & Vavrus, S. J. (2012). Evidence linking Arctic amplification to extreme weather in mid-latitudes. *Geophysical Research Letters*, *39*, L06801. https://doi.org/10.1029/2012GL051000

Gan, B., Wu, L., Jia, F., Li, S., Cai, W., Nakamura, H., et al. (2017). On the response of the Aleutian Low to greenhouse warming. *Journal of Climate*, *30*(10), 3907–3925. https://doi.org/10.1175/JCLI-D-15-0789.1

Goodwin, B. P., Mosley-Thompson, E., Wilson, A. B., Porter, S. E., & Sierra-Hernandez, M. R. (2016). Accumulation variability in the Antarctic Peninsula: The role of large-scale atmospheric oscillations and their interactions. *Journal of Climate*, *29*(7), 2579–2596. https://doi.org/10.1175/JCLI-D-15-0354.1

Holdsworth, G., Fogarasi, S., & Krouse, H. R. (1991). Variation of the stable isotopes of water with altitude in the Saint Elias Mountains of Canada. *Journal of Geophysical Research*, *96*(D4), 7483–7494. https://doi.org/10.1029/91JD00048

Holdsworth, G. H., Krouse, H. R., & Nosal, M. (1992). Ice core climate signals from Mount Logan Yukon A.D. 1700-1987. In R. S. Bradley, & P. D. Jones (Eds.), *Climate since A.D. 1500*, (pp. 483–504). London: Routledge.

Holme, C., Gkinis, V., Lanzky, M., Morris, V., Olesen, M., Thayer, A., et al. (2019). Varying regional δ^{18}O-temperature relationship in high-resolution stable water isotopes from east Greenland. *Climate of the Past*, *15*(3), 893–912. https://doi.org/10.5194/cp-15-893-2019

Hu, F. S., Ito, E., Brown, T. A., Curry, B. B., & Engstrom, D. R. (2001). Pronounced climatic variations in Alaska during the last two millennia. *Proceedings of the National Academy of Sciences of the United States of America*, *98*(19), 10552–10556. https://doi.org/10.1073/pnas.181333798

Huang, B., Banzon, V. F., Freeman, E., Lawrimore, J., Liu, W., Peterson, T. C., et al. (2015). Extended reconstructed sea surface temperature version 4 (ERSST.v4): Part I. Upgrades and intercomparisons. *Journal of Climate*, *28*(3), 911–930. https://doi.org/10.1175/JCLI-D-14-00006.1

Huang, B., Thorne, P. W., Smith, T. M., Liu, W., Lawrimore, J., Banzon, V. F., et al. (2016). Further exploring and quantifying uncertainties for extended reconstructed sea surface temperature (ERSST) version 4 (v4). *Journal of Climate*, *29*(9), 3119–3142. https://doi.org/10.1175/JCLI-D-15-0430.1

Huang, Y., Dong, X., Bailey, D. A., Holland, M. M., Xi, B., DuVivier, A. K., et al. (2019). Thicker clouds and accelerated Arctic sea ice decline: The atmosphere-sea ice interactions in spring. *Geophysical Research Letters*, *46*, 6980–6989. https://doi.org/10.1029/2019GL082791

Hughen, K. A., Overpeck, J. T., & Anderson, R. F. (2000). Recent warming in a 500-year palaeotemperature record from varved sediments, Upper Soper Lake, Baffin Island, Canada. *The Holocene*, *10*(1), 9–19. https://doi.org/10.1191/095968300676746202

Hurley, J. V., Vuille, M., & Hardy, D. R. (2016). Forward modeling of δ^{18}O in Andean ice cores. *Geophysical Research Letters*, *43*, 8178–8188. https://doi.org/10.1002/2016GL070150

Johnsen, S. J. (1977). Stable isotope homogenization of polar firn and ice. *Isotopes and impurities in snow and ice (Proceedings of the Grenoble Symposium August-September 1975)*. International Association of Hydrological Sciences, 118, 210-219.

Johnsen, S. J., Clausen, H. B., Cuffey, K. M., Hoffmann, G., Schwander, J., & Creyts, T. (2000). Diffusion of stable isotopes in polar firn and ice: The isotope effect in firn diffusion. In T. Hondoh (Ed.), *Physics of Ice Core Records*, (pp. 121–140). Sapporo: Hokkaido University Press.

Johnsen, S. J., Dansgaard, W., Clausen, H. B., & Langway, C. C. Jr. (1972). Oxygen isotope profiles through the Antarctic and Greenland ice sheets. *Nature*, *235*(5339), 429–434. https://doi.org/10.1038/235429a0

Jones, P. D., & Mann, M. E. (2004). Climate over past millennia. *Reviews of Geophysics*, *42*, RG2002. https://doi.org/10.1029/2003RG000143

Kaufman, D. S., Axford, Y. L., Henderson, A. C. G., McKay, N. P., Oswald, W. W., Saenger, C., et al. (2016). Holocene climate changes in eastern Beringia (NW North America) – A systematic review of multi-proxy evidence. *Quaternary Science Reviews*, *147*, 312–339. https://doi.org/10.1016/j.quascirev.2015.10.021

Kelsey, E. P., Wake, C. P., Yalcin, K., & Kreutz, K. (2012). Eclipse ice core accumulation and stable isotope variability as an indicator of North Pacific climate. *Journal of Climate*, *25*(18), 6426–6440. https://doi.org/10.1175/JCLI-D-11-00389.1

Kinnard, C., Zdanowicz, C. M., Fisher, D. A., Isaksson, E., de Vernal, A., & Thompson, L. G. (2011). Reconstructed changes in Arctic sea ice over the past 1,450 years. *Nature*, *479*(7374), 509–512. https://doi.org/10.1038/nature10581

Koide, M., Michel, R., Goldberg, E. D., Herron, M. M., & Langway, C. C. Jr. (1982). Characterization of radioactive fallout from pre- and post-moratorium tests to polar ice caps. *Nature*, *296*(5857), 544–547. https://doi.org/10.1038/296544a0

Kosaka, Y., & Xie, S.-P. (2016). The tropical Pacific as a key pacemaker of the variable rates of global warming. *Nature Geoscience*, *9*(9), 669–673. https://doi.org/10.1038/ngeo2770

Kurita, N., Noone, D., Risi, C., Schmidt, G., Yamada, H., & Yoneyama, K. (2011). Intraseasonal isotopic variation associated with the Madden-Julian Oscillation. *Journal of Geophysical Research*, *116*, D24101. https://doi.org/10.1029/2010JD015209

Lachniet, M. S., Lawson, D. E., Stephen, H., Sloat, A. R., & Patterson, W. P. (2016). Isoscapes of δ^{18}O and δ^{2}H reveal climatic forcings on Alaska and Yukon precipitation. *Water Resources Research*, *52*, 6575–6586. https://doi.org/10.1002/2016WR019436

Laepple, T., Munch, T., Casado, M., Hoerhold, M., Landais, A., & Kipfstuhl, S. (2018). On the similarity and apparent cycles of isotopic variations in East Antarctic snow pits. *The Cryosphere*, *12*(1), 169–187. https://doi.org/10.5194/tc-12-169-2018

Lee, H. J., Kwon, M. O., Yeh, S.-W., Kwon, Y.-O., Park, W., Park, W.-H., et al. (2017). Impact of poleward moisture transport from the North Pacific on the acceleration of sea ice loss in the Arctic since 2002. *Journal of Climate*, *30*(17), 6757–6769. https://doi.org/10.1175/JCLI-D-16-0461.1

Lee, J. E., Fung, I., DePaolo, D. J., & Henning, C. C. (2007). Analysis of the global distribution of water isotopes using the NCAR atmospheric general circulation model. *Journal of Geophysical Research*, *112*, D16306. https://doi.org/10.1029/2006JD007657

Liu, J., Zhang, Z., Horton, R. M., Wang, C., & Ren, X. (2007). Variability of North Pacific sea ice and East Asia-North Pacific winter climate. *Journal of Climate*, *20*(10), 1991–2001. https://doi.org/10.1175/JCLI4105.1

Liu, W., Huang, B., Thorne, P. W., Banzon, V. F., Zhang, H.-M., Freeman, E., et al. (2015). Extended reconstructed sea surface temperature version 4 (ERSST.v4): Part II. Parametric and structural uncertainty estimations. *Journal of Climate*, *28*(3), 931–951. https://doi.org/10.1175/JCLI-D-14-00007.1

Masson-Delmotte, V., Steen-Larsen, H. C., Ortega, P., Swingedouw, D., Popp, T., Vinther, B. M., et al. (2015). Recent changes in north-west Greenland climate documented by NEEM shallow ice core data and simulations, and implications for past-temperature reconstructions. *The Cryosphere*, *9*(4), 1481–1504. https://doi.org/10.5194/tc-9-1481-2015

McKay, N. P., & Kaufman, D. S. (2014). An extended Arctic proxy temperature database for the past 2000 years. *Scientific Data*, *1*(1), 140026. https://doi.org/10.1038/sdata.2014.26

Meehl, G. A., Hu, A., Arblaster, J. M., Fasullo, J., & Trenberth, K. (2013). Externally forced and internally generated decadal climate variability associated with the Interdecadal Pacific Oscillation. *Journal of Climate*, *26*(18), 7298–7310. https://doi.org/10.1175/JCLI-D-12-00548.1

Menne, M. J., Durre, I., Vose, R. S., Gleason, B. E., & Houston, T. G. (2012). An overview of the Global Historical Climatology Network-Daily database. *Journal of Atmospheric and Oceanic Technology*, *29*(7), 897–910. https://doi.org/10.1175/JTECH-D-11-00103.1

Mesinger, F., DiMego, G., Kalnay, E., Mitchell, K., Shafran, P. C., Ebisuzaki, W., et al. (2006). North American regional reanalysis. *Bulletin of the American Meteorological Society*, *87*(3), 343–360. https://doi.org/10.1175/BAMS-87-3-343

Midhun, M., & Ramesh, R. (2016). Validation of δ^{18}O as a proxy for past monsoon rain by multi-GCM simulations. *Climate Dynamics*, *46*(5-6), 1371–1385. https://doi.org/10.1007/s00382-015-2652-8

Mock, C. J., Bartlein, P. J., & Anderson, P. M. (1998). Atmospheric circulation patterns and spatial climatic variations in Beringia. *International Journal of Climatology*, *10*, 1085–1104. https://doi.org/10.1002/(SICI)1097-0088(199808)18:10<1085::AID-JOC305>3.0.CO;2-K

Moore, G. W. K., Alverson, K., & Holdsworth, G. (2002). Variability in the climate of the Pacific Ocean and North America as expressed in the Mount Logan ice core. *Annals of Glaciology*, *35*, 423–429. https://doi.org/10.3189/172756402781817185

Moore, G. W. K., Alverson, K., & Holdsworth, G. (2003). The impact that elevation has on the ENSO signal in precipitation records from the Gulf of Alaska region. *Climatic Change*, *59*(1/2), 101–121. https://doi.org/10.1023/A:1024423925161

Moore, G. W. K., Field, R. D., & Benson, C. S. (2016). Impact of source region on the $\delta^{18}O$ signal in snow: A case study from Mount Wrangell, Alaska. *Journal of Hydrometeorology*, *17*(1), 139–151. https://doi.org/10.1175/JHM-D-14-0224.1

Moore, G. W. K., Holdsworth, G., & Alverson, K. (2001). Extra-tropical response to ENSO as expressed in an ice core from the Saint Elias Range. *Geophysical Research Letters*, *28*(18), 3457–3460. https://doi.org/10.1029/2000GL012397

Moore, G. W. K., Holdsworth, G., & Alverson, K. (2002). Climate change in the North Pacific region over the past three centuries. *Nature*, *420*(6914), 401–403. https://doi.org/10.1038/nature01229

Mosley-Thompson, E., McConnell, J. R., Bales, R. C., Li, Z., Lin, P.-N., Steffen, K., et al. (2001). Local to regional-scale variability of Greenland accumulation from PARCA cores. *Journal of Geophysical Research*, *106*(D24), 33839–33851. https://doi.org/10.1029/2001JD900067

National Snow and Ice Data Center (2019). Ho hum February it may be, unless we speak of the Bering Sea. Available at https://nsidc.org/arcticseaicenews/2019/03/ho-hum-february-it-may-be-unless-we-speak-of-the-bering-sea/. Accessed April 23, 2019.

Osterberg, E., Mayewski, P. A., Fisher, D. A., Kreutz, K. J., Maasch, K. A., Sneed, S. B., & Kelsey, E. P. (2014). Mount Logan ice core record of tropical and solar influences on Aleutian Low variability: 500-1998 A.D. *Journal of Geophysical Research: Atmospheres*, *119*, 11,189–11,204. https://doi.org/10.1002/2014JD021847

Osterberg, E. C., Winski, D. A., Kreutz, K. J., Wake, C. P., Ferris, D. G., Campbell, S., et al. (2017). The 1200 year composite ice core record of Aleutian Low intensification. *Geophysical Research Letters*, *44*, 7447–7454. https://doi.org/10.1002/2017GL073697

Overland, J. E., Adams, J. M., & Bond, N. A. (1999). Decadal variability of the Aleutian Low and its relation to high-latitude circulation. *Journal of Climate*, *12*(5), 1542–1548. https://doi.org/10.1175/1520-0442(1999)012<1542:DVOTAL>2.0.CO;2

Overland, J. E., Wood, J. R., & Wang, M. (2011). Warm Arctic—Cold continents: Climate impacts of the newly open Arctic Sea. *Polar Research*, *30*(1), 15787. https://doi.org/10.3402/polar.v30i0.15787

PAGES 2 k Consortium (2013). Continental-scale temperature variability during the past two millennia. *Nature Geoscience*, *6*(5), 339–346. https://doi.org/10.1038/ngeo1797

Porter, T. J., Pisaric, M. F. J., Kokelj, S. V., & deMontigny, P. (2013). A ring-width-based reconstruction of June–July minimum temperatures since AD 1245 from white spruce stands in the Mackenzie Delta region, northwestern Canada. *Quaternary Research*, *80*(2), 167–179. https://doi.org/10.1016/j.yqres.2013.05.004

Rasmussen, S. O., Andersen, K. K., Svensson, A. M., Steffensen, J. P., Vinther, B. M., Clausen, H. B., et al. (2006). A new Greenland ice core chronology for the last glacial termination. *Journal of Geophysical Research*, *111*, D06102. https://doi.org/10.1029/2005JD006079

Richerol, T., Rochon, A., Blasco, S., Scott, D. B., Schell, T. M., & Bennett, R. J. (2008). Evolution of paleo sea-surface conditions over the last 600 years in the Mackenzie Trough, Beaufort Sea (Canada). *Marine Micropaleontology*, *68*(1-2), 6–20. https://doi.org/10.1016/j.marmicro.2008.03.003

Risi, C., Bony, S., Vimeux, F., & Jouzel, J. (2010). Water-stable isotopes in the LMDZ4 general circulation model: Model evaluation for present-day and past climates and applications to climatic interpretations of tropical isotopic records. *Journal of Geophysical Research*, *115*, D12118. https://doi.org/10.1029/2009JD013255

Risi, C., Noone, D., Worden, J., Frankenberg, C., Stiller, G., Kiefer, M., et al. (2012). Process-evaluation of tropospheric humidity simulated by general circulation models using water vapor isotopologues: 1. Comparison between models and observations. *Journal of Geophysical Research*, *117*, D05303. https://doi.org/10.1029/2011JD016623

Rodionov, S. N., Bond, N. A., & Overland, J. E. (2007). The Aleutian Low, storm tracks, and winter climate variability in the Bering Sea. *Deep-Sea Research Part II: Topical Studies in Oceanography*, *54*(23-26), 2560–2577. https://doi.org/10.1016/j.dsr2.2007.08.002

Rolph, G., Stein, A., & Stunder, B. (2017). Real-time Environmental Applications and Display sYstem: READY. *Environmental Modelling & Software*, *95*, 210–228. https://doi.org/10.1016/j.envsoft.2017.06.025

Rupper, S., Stieg, E. J., & Roe, G. (2004). The relationship between snow accumulation at Mt. Logan, Yukon, Canada, and climate variability in the North Pacific. *Journal of Climate*, *17*(24), 4724–4739. https://doi.org/10.1175/JCLI-3202.1

Schmidt, G. A., LeGrande, A. N., & Hoffman, G. (2007). Water isotope expressions of intrinsic and forced variability in a coupled ocean-atmosphere model. *Journal of Geophysical Research*, *112*, D10103. https://doi.org/10.1029/2006JD007781

Screen, J. A., & Francis, J. A. (2016). Contribution of sea-ice loss to Arctic amplification is regulated by Pacific Ocean decadal variability. *Nature Climate Change*, *6*(9), 856–860. https://doi.org/10.1038/nclimate3011

Serreze, M. C., Crawford, A. D., Stroeve, J. C., Barrett, A. P., & Woodgate, R. A. (2016). Variability, trends, and predictability of seasonal sea ice retreat and advance in the Chukchi Sea. *Journal of Geophysical Research: Oceans*, *121*, 7308–7325. https://doi.org/10.1002/2016JC011977

Shindell, D. T., Schmidt, G. A., Mann, M. E., Rind, D., & Waple, A. (2001). Solar forcing of regional climate change during the Maunder Minimum. *Science*, *294*(5549), 2149–2152. https://doi.org/10.1126/science.1064363

Sigl, M., Winstrup, M., McConnell, J. R., Welten, K. C., Plunkett, G., Ludlow, F., et al. (2015). Timing and climate forcing of volcanic eruptions for the past 2,500 years. *Nature*, *523*(7558), 63–66. https://doi.org/10.1038/nature14564

Sime, L. C., Tindall, J. C., Wolff, E. W., Connolley, W. M., & Valdes, P. J. (2008). Antarctic isotopic thermometer during a CO_2 forced warming event. *Journal of Geophysical Research*, *113*, D24119. https://doi.org/10.1029/2008JD010395

Sjolte, J., Hoffman, G., Johnsen, S. J., Vinther, B. M., Masson-Delmotte, V., & Sturm, C. (2011). Modeling the water isotopes in Greenland precipitation 1959-2001 with the meso-scale model REMO-iso. *Journal of Geophysical Research*, *116*, D18105. https://doi.org/10.1029/2010JD015287

Stafford, J. M., Wendler, G., & Curtis, J. (2000). Temperature and precipitation of Alaska: 50 year trend analysis. *Theoretical and Applied Climatology*, *67*(1-2), 33–44. https://doi.org/10.1007/s007040070

Steen-Larsen, H. C., Masson-Delmotte, V., Sjolte, J., Johnsen, S. J., Vinther, B. M., Bréon, F.-M., et al. (2011). Understanding the climatic signal in the water stable isotope records from the NEEM shallow firn/ice cores in northwest Greenland. *Journal of Geophysical Research*, *116*, D06108. https://doi.org/10.1029/2010/JD014311

Steen-Larsen, H. C., Risi, C., Werner, M., Yoshimura, K., & Masson-Delmotte, V. (2017). Evaluating the skills of isotope-enabled general circulation models against in situ atmospheric water vapor isotope observations. *Journal of Geophysical Research: Atmospheres*, *122*, 246–263. https://doi.org/10.1002/2016JD025443

Stein, A. F., Draxler, R. R., Rolph, R. D., Stunder, B. J. B., Cohen, M. D., & Ngan, F. (2015). NOAA's HYSPLIT atmospheric transport and dispersion modeling system. *Bulletin of the American Meteorological Society*, *96*(12), 2059–2077. https://doi.org/10.1175/BAMS-D-14-00110.1

Streten, N. A. (1974). Some features of the summer climate of interior Alaska. *Journal of the Arctic Institute of North America*, *27*(4), 273–286. https://doi.org/10.14430/arctic2884

Szeicz, J. M., & MacDonald, G. M. (1995). Dendroclimatic reconstruction of summer temperatures in Northwestern Canada since A.D. 1638 based on age-dependent modeling. *Quaternary Research*, *44*(2), 257–266. https://doi.org/10.1006/qres.1995.1070

Tinner, W., Bigler, C., Gedye, S., Gregory-Eaves, I., Jones, R. T., Kaltenreider, P., et al. (2008). A 700-year paleoecological record of boreal ecosystem responses to climatic variation from Alaska. *Ecology*, *89*(3), 729–743. https://doi.org/10.1890/06-1420.1

Urmann, D. (2009). Decadal scale climate variability during the last millennium as recorded by the Bona-Churchill and Quelccaya ice cores, (Doctoral dissertation). Retrieved from OhioLink. (http://rave.ohiolink.edu/etdc/view?acc_num=osu1237853800). Columbus, OH: The Ohio State University.

Wake, C. P., Yalcin, K., & Gundestrup, N. S. (2002). The climate signal recorded in the oxygen-isotope, accumulation and major-ion time series from the Eclipse ice core, Yukon Territory, Canada. *Annals of Glaciology*, *35*, 416–422. https://doi.org/10.3189/172756402781817266

Whittaker, L. M., & Horn, L. H. (1984). Northern Hemisphere extratropical cyclone activity for four mid-season months. *Journal of Climatology*, *4*(3), 297–310. https://doi.org/10.1002/joc.3370040307

Wiles, G. C., D'Arrigo, R. D., Villabla, R., Calkin, P. E., & Barclay, D. J. (2004). Century-scale solar variability and Alaskan temperature change over the past millennium. *Geophysical Research Letters*, *31*, L15203. https://doi.org/10.1029/2004GL020050

Wilson, R., Wiles, G., D'Arrigo, R., & Zweck, C. (2007). Cycles and shifts: 1300 years of multi-decadal temperature variability in the Gulf of Alaska. *Climate Dynamics*, *28*(4), 425–440. https://doi.org/10.1007/s00382-006-0194-9

Winski, D., Osterberg, E., Ferris, D., Kreutz, K., Wake, C., Campbell, S., et al. (2017). Industrial-age doubling of snow accumulation in the Alaska Range linked to tropical ocean warming. *Scientific Reports*, *7*, 17869. https://doi.org/10.1038/s41598-017-18022-5

Woodgate, R. A. (2018). Increases in the Pacific inflow to the Arctic from 1990 to 2015, and insights into seasonal trends and driving mechanisms from year-round Bering Strait mooring data. *Progress in Oceanography*, *160*, 124–154. https://doi.org/10.1016/j.pocean.2017.12.007

Woodgate, R. A., Aagaard, K., & Weingartner, T. J. (2005). Monthly temperature, salinity, and transport variability of the Bering Strait through flow. *Geophysical Research Letters*, *32*, L04601. https://doi.org/10.1029/2004GL021880

Woodgate, R. A., Weingartner, T. J., & Lindsay, R. W. (2010). The 2007 Bering Strait oceanic heat flux and anomalous Arctic sea-ice retreat. *Geophysical Research Letters*, *37*, L01602. https://doi.org/10.1029/2009GL041621

Yoshimura, K., Kanamitsu, M., Noone, D., & Oki, T. (2008). Historical isotope simulation using reanalysis atmospheric data. *Journal of Geophysical Research*, *113*, D19108. https://doi.org/10.1029/2008JD010074

Zielinski, G. A. (1995). Stratospheric loading and optical depth estimates of explosive volcanism over the last 2100 years derived from the GISP2 Greenland ice core. *Journal of Geophysical Research*, *100*, 20937–20955. https://doi.org/10.1029/95JD01751